


The impact of different corona models on FD algorithms for the solution of multiconductor transmission lines equations

Erika Stracqualursi¹ | Rodolfo Araneo¹  | Amedeo Andreotti²

¹DIAEE—Electrical Engineering Division, University of Rome “La Sapienza”, Rome, Italy

²Electrical Engineering Department, University Federico II of Napoli, Napoli, Italy

Correspondence

Rodolfo Araneo, DIAEE—Electrical Engineering Division, University of Rome “La Sapienza”, Via Eudossiana 18, 00184 Rome, Italy.
Email: rodolfo.araneo@uniroma1.it

Associate Editor: Xingming Bian

Abstract

In this study, the implementation of different corona discharge models in a transient program for overhead multiconductor lines based on the implicit Crank-Nicolson Finite Difference Time Domain method is presented. Among different corona models available in the literature, two empirical models (Gary's and Suliciu's models) and a physics-based model (Malik's model) are discussed, which are broadly used in EMT programs, and their predictions under fast-front lightning surges and slow-front switching impulses are assessed. The authors critically review the dynamic capacitance approach in terms of numerical accuracy, when dealing with slowly varying voltages, and applicability, regarding dispersive models assuming a non-instantaneous charge-voltage relation. The alternative voltage-controlled generator approach is proposed, which is successfully included in the implicit Crank-Nicolson scheme. One of the objectives of this study is to show how different corona models may predict overvoltages with huge discrepancies, depending on the transient waveform and the propagation distance, despite the similarity of the q - v hysteresis curves. More evident discrepancies between models under fast-front voltage waves are reported, rather than for switching impulses. The consistency of these results in terms of the models' features and q - v curves is analysed, highlighting the necessity for new engineering tools for corona simulation of general predictive capability.

1 | INTRODUCTION

Assessment of overvoltages in high-voltage overhead power lines is essential for both sizing of components and insulation coordination [1]. Propagation of internal or external surges, and especially those due to direct or indirect lightning strokes [2, 3], is strongly affected by non-uniformities (e.g. periodic grounding of shield wires [4]), frequency-dependent losses (e.g. resistive earth-return path [5, 6]), and non-linearities (e.g. corona phenomenon [7]). Due to the pioneering works of Peek [8] and the experimental data of Wagner [9], corona was recognised as a key phenomenon in high-voltage engineering.

It was immediately apparent that it causes additional attenuation and distortion on travelling surges and is responsible for power losses, and secondary yet detectable effects, such as noise [10] and interference with communication lines, especially when the ionisation process has developed to the so-called visible corona [11]. Corona effect is a well-known effect

due to a non-linear discharge mechanism that occurs when the electric field intensity reaches a critical inception value. Above this value, air surrounding the conductor is subject to an ionisation process, beginning to be converted into ozone, and a complex streamer breakdown mechanism [12] gives rise to transversal currents confined into the corona region where a space-charge is injected by the streamer activity. The corona effect is responsible for an increase in the per unit length (p.u.l.) capacitance, for a decrease in surge propagation velocity and adds losses that generally lead to extra damping during the wave propagation [13]. Since the phenomenon is non-linear and characterised by a hysteretic q - v loop, a dynamic, non-linear and time-varying capacitance [14] is generally introduced to replace the standard geometric capacitance.

In dealing with non-uniformities and distributed non-linearities, like in the case of corona, it is known that well-established methods based on the frequency domain analysis of the multiconductor transmission lines (MTLs) and the

This is an open access article under the terms of the Creative Commons Attribution License, which permits use, distribution and reproduction in any medium, provided the original work is properly cited.

© 2021 The Authors. *High Voltage* published by John Wiley & Sons Ltd on behalf of The Institution of Engineering and Technology and China Electric Power Research Institute.

inverse Fourier transform of the results cannot be used. Consequently, tools based on time-domain approaches must be the preferred choice, allowing for accounting of the above phenomena. Anyway, the inclusion of the corona phenomenon in any commercial or customised tool [15] relies on the choice of the particular model that is used to reproduce this extremely complex behaviour. Corona depends on many factors, such as atmospheric conditions, temperature, air density, humidity [16], and on the conductor's geometry, including the roughness of the surface [17] etc. Moreover, it is essential to distinguish between d.c. corona [18], a.c. corona, impulse corona, and corona under oscillating surges [19]. Several techniques have been proposed in the literature to model the corona phenomenon and they can be broadly classified into two approaches.

The first approach relies on the development of sophisticated mathematical tools that try to translate the corona physical mechanism in a set of non-linear equations, able to reproduce the q - v curve under any applied voltage waveform. Still today, it is questionable to what extent these methods can predict the real corona mechanism under any transient. These methods ask for the tuning of several parameters, usually on a trial-and-error optimisation process, to fit measured data. Among these methods, it is worthy to cite models by Malik et al. [17], Cooray [20], Correia de Barros [21], and more recently Huang et al. [22], which account, with different degrees of accuracy, for all the most important mechanisms (i.e. surface charge, space-charge, time lag, critical electric field, back corona effect etc.).

A second kind of technique is based on experimental tests carried out on the charge-voltage characteristics: an approximation is generally proposed to describe the variation of the corona dynamic capacitance. Although these methods are relatively simple and easy to use in tools that can treat transients, they are widely used till today [7], and their applicability poses several subtle issues. They enforce the trend and characteristics of the corona dynamic capacitance beforehand, and this seems incorrect and inappropriate [23], since the resulting trend should be affected by the voltage waveform. Some of them introduce a voltage-dependent conductance in parallel to the dynamic capacitance to account for corona losses; however, corona losses are given by the area of the q - v loop and, in turn, are non-linear and dependent on several parameters. Popular models are those proposed by Gary [24], Suliciu [25], Inoue [23], Sivaev and Podporkin [26], Skilling [27] and Umoto [28].

A particular subset of this second approach is characterised by simplified circuit models aimed at representing the corona non-linear dynamic capacitance and conductance along a line conductor. An equivalent circuit model was initially proposed by J. Martí [29]; later models have been proposed by Lee [30], Maruvada [31], Motoyama and Ametani [32], and Maccioni [33].

The proposed study investigates the suitability of different corona models, particularly in view of their inclusion in tools for the transient analysis. To this aim, after a preliminary review and comparison of some of the aforementioned available models, we address their implementation into a transient

program based on the Finite Difference Time Domain (FDTD) technique. The results show that prior adjustment of the parameters required by each model to give similar q - v curves may still bring to different results along the line, highlighting the necessity for a new versatile engineering tool modelling corona. On the other hand, the study questions the general applicability and the smoothness in numerical implementation of the traditional dynamic capacitance approach, proposing a stable, yet numerically friendly, solution for the inclusion of this strong non-linear phenomenon in FDTD codes. Distributed voltage-controlled current generators are proposed to account for corona, and implemented in an implicit Crank-Nicolson time-stepping scheme [34]. This scheme may ease several sources of numerical instabilities characterising the explicit leap-frog scheme [35] and is suitable for parallelisation [36].

The remainder of the paper is organised as follows: in Section 2, we briefly recall the mechanism of corona inception and discharge; Section 3 covers, in detail, the inclusion of the corona phenomenon in the FDTD implicit scheme; in Section 4, models selected for implementation have been examined and reviewed. Finally, the results computed for the propagation of voltage waves with corona, and conclusions, along with future developments of the research are presented in Sections 5 and 6, respectively.

2 | BASIC ASSUMPTIONS ON CORONA INCEPTION AND DEVELOPMENT

Let us consider a single conductor of radius r_0 at height h over the ground. The electric discharge starts on the conductor surface at r_0 , where the electric field $e_0(t)$ is the highest. With reference to Figure 1, where the hysteretic q - v curve is shown, experimental evidence show that the corona discharge starts at point A, as $e_0(t)$ reaches and overcomes the critical inception electric field E_{inc} of the insulating air, dependent on current atmospheric conditions (pressure, humidity and temperature). This value is meant as a threshold in a statistical sense; that is, the value at 50% of probability of a local discharge inception. Several approaches are available in the literature for the computation of E_{inc} [37, 38]; however, being the accurate physical analysis of corona out of the scope of the present work, we will refer to the simple and common expression of E_{inc} , expressed in kV/cm (Peek [8]):

$$E_{inc} = 30 m \delta f_p \left(1 + \frac{0.3}{\sqrt{\delta r_{0cm}}} \right), \quad (1)$$

where m is the surface irregularity factor (in the range between 0.72 and 0.82), δ is the relative air density (herein it is set equal to 1 that is an adequate value for fair weather) that takes into account the influence on the visual corona critical field due to different temperature or barometric pressure; f_p is the polarity factor of the voltage surges (approximately equal to 0.5 for positive polarity and equal to 1 for negative one [17]); r_{0cm} is

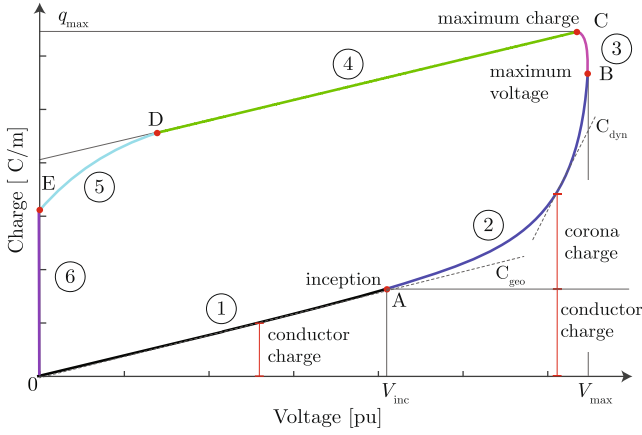


FIGURE 1 Trend of a hysteretic $q-v$ curve

the wire radius expressed in centimetres. From Equation (1), the critical inception voltage may be obtained as follows:

$$V_{\text{inc}} = E_{\text{inc}} r_0 \frac{2b - r_0}{2b} \ln\left(\frac{2b - r_0}{r_0}\right) \approx E_{\text{inc}} r_0 \ln\left(\frac{2b}{r_0}\right). \quad (2)$$

The corona phenomenon is ruled by the electric field: as long as $e_0(t)$ on the conductor surface is below the inception value E_{inc} (equivalently, the voltage $v(t)$ of the conductor is below V_{inc}), no corona effect takes place and the p.u.l. charge $q(t)$ and the voltage $v(t)$ are linked through the p.u.l. geometric capacitance C_{geo} (part ① of the curve). A further increase of the voltage $v(t)$ over V_{inc} leads to an electric field $e_0(t) > E_{\text{inc}}$, causing the inception of corona on the conductor surface and the subsequent phenomenon of partial discharges in air; the charge $q(t)$ and the voltage $v(t)$ are now linked through a p.u.l. dynamic time-dependent non-linear capacitance $C_{\text{dyn}}(t)$ (part ② of the curve). Generally, the total transversal current i_t (expressed in A/m) drained towards the ground may be computed as the time derivative of the p.u.l. charge on the conductor:

$$i_t = i_{\text{geo}} + i_{\text{co}} = \frac{dq}{dt} = \frac{dq}{dv} \frac{dv}{dt} = C_{\text{dyn}}(t) \frac{dv}{dt}, \quad (3)$$

where i_{geo} is the capacitive current associated with the line geometry, and i_{co} is the additional contribute due to the corona over-charge. In Equation (3), in the absence of corona, $i_{\text{co}} = 0$, and $C_{\text{dyn}}(t) = C_{\text{geo}}$.

A delay time τ is needed for space-charge to build up in the corona cloud around the conductor due to impressed voltage. This is visible and measurable in part ③ of the curve: after the voltage reaches its peak value (at time t_v^{max}) and starts to decrease, the charge q continues to increase until reaching its peak (at time t_q^{max}). The delay time τ is defined as $t_q^{\text{max}} - t_v^{\text{max}}$: it is assumed to be constant although, very likely, it is described by some non-linear function of $v(t)$.

The non-linear relation between charge and voltage prevents the possibility of addressing the study in the frequency domain; on the contrary, the finite difference time domain

(FDTD) analysis allows to study corona, even though the problem is twofold.

First, it is necessary to select the proper corona model for the accurate simulation of the non-linear phenomenon. In practice, C_{dyn} strongly depends on the surge waveform, polarity, peak value, and time scale; consequently, the model should be able to reproduce the $q-v$ relation under different transient conditions.

Additionally, the hysteretic behaviour of the $q-v$ loop translates in a multivalued dependence of the charge on the applied voltage $v(t)$, which deserves attention for the accurate inclusion of losses. Several models assume C_{dyn} is equal to C_{geo} in the descending branch of the $q-v$ curve, as the sign of dv/dt is reversed (part ④ of the curve). However, mostly when r_0 is large, a point D exists where the electric field due to charge on conductor is no longer prevalent compared to that generated by space-charge; hence, free corona space-charge decreases in a much faster rate.

Finally, all models end at point E, which represents the free residual space-charge in the corona cloud when the voltage has reached a null value. Anyway, the space-charges would progressively fade after the time necessary to their drift and recombination.

3 | IMPLEMENTATION OF CORONA IN AN IMPLICIT FDTD ALGORITHM

In the present section, we address the inclusion of corona in a FDTD scheme for multiconductor lines. Due to its intrinsic stability, the implicit Crank-Nicolson updating scheme is particularly suitable for the study of waves propagating along MTLs in the presence of corona; when dealing with propagation, corona may be identified as a non-linearity of the system, and also as an additional non-uniformity, since it may develop at different sections of the line, depending on the instantaneous value of the voltage.

For a MTL with N_w conductors, assumed to be at an average height above a lossy ground, the Time-Domain Telegraphers Equations in the absence of corona read [39]

$$-\frac{\partial \mathbf{v}(x, t)}{\partial x} = \int_0^t \boldsymbol{\zeta}(t - \tau) \frac{\partial \mathbf{i}}{\partial \tau} d\tau + \mathbf{L}_{\text{ext}} \frac{\partial \mathbf{i}(x, t)}{\partial t} \quad (4)$$

$$-\frac{\partial \mathbf{i}(x, t)}{\partial x} = \mathbf{C} \frac{\partial \mathbf{v}(x, t)}{\partial t} + \mathbf{G} \mathbf{v}(x, t), \quad (5)$$

where $\mathbf{i}(x, t)$ and $\mathbf{v}(x, t)$ are the $N_w \times 1$ vectors of voltages-to-ground and currents of wires; τ is the integration variable of the convolution integral evaluated at time t ; \mathbf{L}_{ext} and \mathbf{C} are the $N_w \times N_w$ matrices of p.u.l. external inductance and capacitance, set equal to the matrix of geometric capacitances in the absence of corona, or to \mathbf{C}_{dyn} (to which reference is made in Section 3.1) when corona occurs. $\boldsymbol{\zeta}(t)$ is the matrix of the p.u.l. transient impedance, which is generally introduced in the time domain to include the frequency-dependent longitudinal losses distributed into ground and internal to wires [40]. The p.u.l. conductance \mathbf{G} should take into account transversal losses; however, \mathbf{G} , which is

usually associated with corona effect, is here taken into account by means of the hysteretic corona behaviour.

Extensive considerations regarding numerical dispersion and advantages in terms of stability of the Crank-Nicolson scheme, here excluded for conciseness, may be found in [41]. We denoted with Δx and Δt , the space and time step, respectively, and with $k\Delta x$ and $n\Delta t$, the space-time coordinates of a voltage node along the line at a distance $k\Delta x$ from the MTL left termination; the total number of voltage nodes is $N_x + 1$. Fundamental equations of the implicit scheme read, for a lossless MTL:

First explicit sub-step

$$-\frac{v_{k+1}^n - v_k^n}{\Delta x} = \mathbf{L}_{\text{ext}} \frac{i_{k+\frac{1}{2}}^{n+\frac{1}{2}} - i_{k-\frac{1}{2}}^n}{\Delta t/2} \quad (6)$$

$$-\frac{i_{k+\frac{1}{2}}^n - i_{k-\frac{1}{2}}^n}{\Delta x} = \mathbf{C} \frac{v_k^{n+\frac{1}{2}} - v_k^n}{\Delta t/2}, \quad (7)$$

Second implicit sub-step

$$-\frac{v_{k+1}^{n+1} - v_k^{n+1}}{\Delta x} = \mathbf{L}_{\text{ext}} \frac{i_{k+\frac{1}{2}}^{n+1} - i_{k-\frac{1}{2}}^{n+\frac{1}{2}}}{\Delta t/2} \quad (8)$$

$$-\frac{i_{k+\frac{1}{2}}^{n+1} - i_{k-\frac{1}{2}}^{n+1}}{\Delta x} = \mathbf{C} \frac{v_k^{n+1} - v_k^{n+\frac{1}{2}}}{\Delta t/2}. \quad (9)$$

Subscripts k , $k+1$ of \mathbf{v} denote the subsequent nodes limiting adjacent line sections (of length Δx) at which the voltage is computed; subscripts $k-1/2$, $k+1/2$ of \mathbf{i} refer to the currents entering and leaving the voltage node denoted with k , respectively. Starting from values at time $n\Delta t$, the unknown vectors of voltages \mathbf{v}^{n+1} and currents \mathbf{i}^{n+1} for every node at time $(n+1)\Delta t$ are computed splitting the time step in two sub-steps $\Delta t/2$ long: first, voltages and currents are computed explicitly at $(n+1/2)\Delta t$ from relations (6) and (7); then, implicit Equations (8) and (9) need to be solved in the unknowns.

Summation of Equations (6) and (7) with (8) and (9), respectively, (in the current form, they would be only valid for a lossless MTL) and introduction of the integral term appearing in Equation (4) gives

$$-\frac{1}{2} \left(\frac{v_{k+1}^{n+1} - v_k^{n+1}}{\Delta x} + \frac{v_{k+1}^n - v_k^n}{\Delta x} \right) = \quad (10)$$

$$= \mathbf{L}_{\text{ext}} \frac{i_{k+\frac{1}{2}}^{n+1} - i_{k-\frac{1}{2}}^n}{\Delta t} + \mathbf{C} \mathbf{I}_{k+\frac{1}{2}}^{n+\frac{1}{2}} + \Delta \mathbf{C} \mathbf{I}_{k+\frac{1}{2}}^{n+\frac{1}{2}}$$

$$-\frac{1}{2} \left(\frac{i_{k+\frac{1}{2}}^{n+1} - i_{k-\frac{1}{2}}^{n+1}}{\Delta x} + \frac{i_{k+\frac{1}{2}}^n - i_{k-\frac{1}{2}}^n}{\Delta x} \right) = \quad (11)$$

$$= \mathbf{C} \frac{v_k^{n+1} - v_k^n}{\Delta t}.$$

where terms $\mathbf{C} \mathbf{I}_{k+\frac{1}{2}}^{n+\frac{1}{2}}$ and $\Delta \mathbf{C} \mathbf{I}_{k+\frac{1}{2}}^{n+\frac{1}{2}}$ are introduced to take into account frequency-dependent internal impedance of the wires and impedance offered by the ground return path at time $t = (n+1/2)\Delta t$. These terms may be derived by suitable manipulation of the integral in the right-hand side of Equation (4) performed between 0 and $(n+1/2)\Delta t$, which is here repeated for clarity:

$$\mathbf{C} \mathbf{I}_{\text{tot}}^{n+\frac{1}{2}} = \int_0^{t^*} \boldsymbol{\zeta}(t^* - \tau) \frac{\partial \mathbf{i}}{\partial \tau} d\tau = \mathbf{C} \mathbf{I}_{k+\frac{1}{2}}^{n+\frac{1}{2}} + \Delta \mathbf{C} \mathbf{I}_{k+\frac{1}{2}}^{n+\frac{1}{2}}, \quad (12)$$

where $t^* = (n+1/2)\Delta t$, and the space collocation at $x = (k+\frac{1}{2})\Delta x$ of $\mathbf{C} \mathbf{I}_{\text{tot}}^{n+\frac{1}{2}}$ has been dropped to simplify the notation. From the right-hand side of Equation (12), $\mathbf{C} \mathbf{I}_{\text{tot}}^{n+\frac{1}{2}}$ can be computed as the sum of the two following terms:

$$\mathbf{C} \mathbf{I}_{k+\frac{1}{2}}^{n+\frac{1}{2}} = \int_0^{(n-1/2)\Delta t} \boldsymbol{\zeta}(t^* - \tau) \frac{\partial \mathbf{i}}{\partial \tau} d\tau \quad (13)$$

$$\Delta \mathbf{C} \mathbf{I}_{k+\frac{1}{2}}^{n+\frac{1}{2}} = \int_{(n-1/2)\Delta t}^{(n+1/2)\Delta t} \boldsymbol{\zeta}(t^* - \tau) \frac{\partial \mathbf{i}}{\partial \tau} d\tau. \quad (14)$$

Employing a recursive evaluation of the transient impedances based on Prony approximation, $\mathbf{C} \mathbf{I}_{k+\frac{1}{2}}^{n+\frac{1}{2}}$ is the *history* integral, which is directly derived by updating $\mathbf{C} \mathbf{I}_{\text{tot}}^{n-\frac{1}{2}}$ (the interested reader may find further details in [6]); instead, $\Delta \mathbf{C} \mathbf{I}_{k+\frac{1}{2}}^{n+\frac{1}{2}}$ may be computed through the trapezoidal rule of integration as follows:

$$\Delta \mathbf{C} \mathbf{I}_{k+\frac{1}{2}}^{n+\frac{1}{2}} = \frac{\boldsymbol{\zeta}(0)}{2} (\mathbf{i}_{k+\frac{1}{2}}^{n+1} - \mathbf{i}_{k+\frac{1}{2}}^n) + \frac{\boldsymbol{\zeta}(\Delta t)}{2} (\mathbf{i}_{k+\frac{1}{2}}^n - \mathbf{i}_{k+\frac{1}{2}}^{n-1}). \quad (15)$$

Algebraic manipulation and rearrangement of Equations (10) and (11) lead to the following linear system [41]:

$$\mathbf{A} \mathbf{X}^{n+1} = \mathbf{B}^{n+1} \quad (16)$$

with

$$\mathbf{X}^{n+1} = \begin{bmatrix} \mathbf{v}_0^{n+1} & \mathbf{i}_{\frac{1}{2}}^{n+1} & \mathbf{v}_1^{n+1} & \dots & \mathbf{v}_{N_x}^{n+1} \end{bmatrix} \quad (17)$$

$$\mathbf{B}^{n+1} = \begin{bmatrix} \mathbf{B}_0^V & \mathbf{B}_{\frac{1}{2}}^I & \mathbf{B}_1^V & \dots & \mathbf{B}_{N_x}^V \end{bmatrix}. \quad (18)$$

$\mathbf{v} \mathbf{X}^{n+1}$ is the $(2N_x + 1) \times 1$ vector of the unknowns along the line; \mathbf{B}^{n+1} , of dimension $(2N_x + 1) \times 1$, is the known terms vector of the linear system, which is built by alternation of the known terms vectors of Equations (11) and (10) (denoted with superscripts V and I, respectively). Choice of alternating equations in unknown voltages and currents at each node, as in Equations (17) and (18), allows the coefficient matrix \mathbf{A} in Equation (16) to be a block tri-diagonal matrix, whose square blocks are of order N_w and band is $2N_w - 1$ wide, with an advantage in terms of computational efficiency.

3.1 | Dynamic capacitance approach

Additional dumping of travelling voltage waves, along with reduction of propagation velocity associated with corona discharge, may be taken into account through the matrix \mathbf{C}_{dyn} in place of \mathbf{C} . Conductors-to-ground voltages at time $(n+1)\Delta t$, computed through the solution of the linear system (16), are employed to assess any inception or further development of corona for each conductor of the MTL.

After the selection of a model suitable for the simulation of corona, the dynamic capacitance $C_{\text{dyn}_j}^{n+1,k}$ of conductor j at time $(n+1)\Delta t$ and at $k\Delta x$ (with $j = 1 \dots N_w$, and $k = 0 \dots N_x$) may be evaluated as the function of the corresponding voltage v , starting from the time derivative of the p.u.l. charge q_j associated with conductor j :

$$\frac{dq_j(v)}{dt} = \frac{dq_j(v)}{dv} \frac{dv(t)}{dt} = C_{\text{dyn}_j} \frac{dv(t)}{dt}, \quad (19)$$

with $C_{\text{dyn}_j} = dq_j(v)/dv$.

At each $k\Delta x$, the matrix of dynamic capacitances $\mathbf{C}_{\text{dyn}}^{n+1,k}$ may be computed by inversion of the matrix of potential coefficients $\mathbf{P}^{n+1,k}$, whose diagonal elements are modified according to the degree of development of corona discharge for each conductor (when its voltage overcomes the corresponding inception value):

$$\text{diag}(\mathbf{P}^{n+1,k}) = \left[1/C_{\text{dyn}_1}^{n+1,k} \quad 1/C_{\text{dyn}_2}^{n+1,k} \quad \dots \quad 1/C_{\text{dyn}_{N_w}}^{n+1,k} \right]. \quad (20)$$

The updated $\mathbf{C}_{\text{dyn}}^{n+1,k}$ may be plugged into Equations (6)–(9), for the solution of the subsequent time step, starting from time $(n+1)\Delta t$ to evaluate unknown voltages and currents at time $(n+2)\Delta t$.

However, the computation of the dynamic capacitances matrix introduces an additional computational cost due to the inversion of the modified matrix of potential coefficients, when at least one of the conductors is showing corona; even more important, although the implementation of \mathbf{C}_{dyn} represents a frequently adopted approach in the literature [42] (also in indirect lightning studies [43]), it lacks generality since capacitance, as a circuital element should account for the instantaneous (i.e. local) relationship between voltage and charge, while some corona models (e.g. [17, 21]) assume the p. u.l. charge to depend not only on the instantaneous conductor-to-ground voltage, but also on the voltage past values, which influence charge formation after a delay time τ .

Furthermore, evaluation of the charge derivative in Equation (3) through its corresponding FD form, whether it is computed by a two-point or multiple-point differentiation formula, is a difficult task to be performed with accuracy: from a practical point of view, intervals with weakly ringing, slowly varying or constant voltage may lead to an undeterminate numerical form of the ratio dq/dv , which is not easy to treat

numerically with sufficient accuracy, also due to numerical noise.

3.2 | Voltage-controlled current generator approach

For the reasons mentioned above, the authors have chosen an alternative and general approach, including corona through a voltage-controlled current generator in parallel with the p.u.l. geometric capacitance of the conductors. Therefore, Equation (11) would turn into the following:

$$\begin{aligned} & -\frac{1}{2} \left(\frac{\mathbf{i}_{k+\frac{1}{2}}^{n+1} - \mathbf{i}_{k-\frac{1}{2}}^{n+1}}{\Delta x} + \frac{\mathbf{i}_{k+\frac{1}{2}}^n - \mathbf{i}_{k-\frac{1}{2}}^n}{\Delta x} \right) \\ & = \mathbf{C} \frac{\mathbf{v}_k^{n+1} - \mathbf{v}_k^n}{\Delta t} + \mathbf{i}_{\text{co}}^{n,k}, \end{aligned} \quad (21)$$

where $\mathbf{i}_{\text{co}}^{n,k}$ represents the vector of transversal currents exiting from each conductor due to corona discharge at time $n\Delta t$, employed for the computation of the unknowns at time $(n+1)\Delta t$.

4 | CORONA MODELS FOR FD ANALYSIS

Three different corona models available in the literature have been chosen to simulate corona effects through the implicit FDTD updating scheme. In particular, among the large variety of models available in the literature, we will refer to Malik's model [17], Gary's model [24], and Suliciu's model [25]. While Gary's and Suliciu's empirical models have been chosen since they are among the most widely applied models in the literature, Malik's model is considered for its attempt of reproducing the phenomenon starting from physical considerations. In the current section, a brief overview of these models, along with the description of the equations for computing i_{co} through each model will be performed.

4.1 | Malik's model

This model adopts a simplified and macroscopic description of the physical mechanisms underlying the corona phenomenon, which would require a coupled electro-fluid dynamic plasma model to be fully determined [44], conflicting to formulate simple tools suitable for engineering purposes.

In this model [17], as long as the voltage $v(t)$ is greater than V_{inc} , the dynamic behaviour of corona is simulated through an apparent increase of the conductor radius r_0 , which is replaced by the radius $r_c(t) \geq r_0$. The latter corresponds to the external boundary of the whole space-charge around the conductor.

The model assumes a time delay τ (ranging between $0.1 \mu\text{s}$ and $0.5 \mu\text{s}$) in the formation of corona charge for the instantaneous value of the voltage applied to the conductor. The time-dependent p.u.l. total charge $q(t)$ is given by

$$q(t) = 2\pi\epsilon_0\alpha E_{\text{inc}} r_c(t) \frac{2b - r_c(t)}{2b} + C_{\text{geo}}[v(t) - v(t - \tau)], \quad (22)$$

where ϵ_0 is the vacuum permittivity, and the radius $r_c(t)$ in the presence of corona can be determined by solving the following non-linear equation at each time instant t

$$r_c(t) \left\{ 1 + \frac{2b - r_c(t)}{2b} \ln \left[\frac{2b - r_c(t)}{r_c(t)} \right] \right\} = r_0 + \frac{v(t - \tau)}{\alpha E_{\text{inc}}}. \quad (23)$$

In Equations (22) and (23), $\alpha < 1$ is a multiplicative factor taking into account the reduction of the electric field in the corona area after the inception, assumed constant and equal to αE_{inc} inside the corona sheath; consequently, the surface electric field $e_0(t)$ undergoes an abrupt discontinuity when the corona discharge starts, which can result in discontinuity of $q-v$ relation. Comparison with Equation (2) shows that the parameter α introduces a step discontinuity between r_0 and $r_c(t)$ at t_{inc} ; the lower is α , the larger is the step discontinuity and the wider is the resulting corona hysteretic loop. Along with τ , this is the main parameter to be tuned for optimal fitting of measured results.

Additional corona current in Equation (21) is further specified here, starting from the time derivative of the p.u.l. total charge in Equation (22):

$$i_t(t) = \frac{dq(v(t), v(t - \tau))}{dt} = \frac{dq}{dv(t)} \frac{dv(t)}{dt} + \frac{dq}{dv(t - \tau)} \frac{dv(t - \tau)}{dt}. \quad (24)$$

Considering r_c in Equation (23) as a function of $v(t - \tau)$, that is, $r_c(t) = r_c(v(t - \tau))$, the corona current i_{co} for $dv(t)/dt > 0$ is computed from Equations (22)–(24) as follows:

$$i_{\text{co}}(t) = i_t(t) - i_{\text{geo}}(t) = \frac{2\pi\epsilon_0}{\log\left(\frac{2b - r_c(t)}{r_c(t)}\right)} \frac{dv(t - \tau)}{dt} - C_{\text{geo}} \frac{dv(t - \tau)}{dt}. \quad (25)$$

As the maximum charge is reached and the voltage $v(t)$ decreases, the additional current generator is switched off, and charge and voltage are linked by the geometric capacitance C_{geo} .

4.2 | Gary's model

Starting from experimental $q-v$ curves, this empirical model originally provided an expression of the p.u.l. charge as a function of the conductor voltage $q(v)$ [24]. The value of the voltage-controlled current generator i_{co} for each conductor entering corona along the line to be plugged into Equation (21) is computed as follows:

$$i_{\text{co}}(t) = C_{\text{geo}} \left[B \left(\frac{v(t)}{V_{\text{inc}}} \right)^{B-1} - 1 \right] \frac{dv(t)}{dt}, \quad (26)$$

where the coefficient B is given by the following experimental formula to fit measured data, differentiating between impulses of opposite polarity:

$$B = \begin{cases} 2.924r_0^{0.153} & \text{positive polarity} \\ 1.121 + 6.8r_0 & \text{negative polarity.} \end{cases} \quad (27)$$

The parameters in Equation (27) have been found for a variety of conductors diameters (ranging between 1 and 6.5 cm) and impressed voltage impulses (from 1.2/50 to 250/2500 μs) [24]. As for Malik's model, i_{co} is switched off when sweeping the descending branch of the $q-v$ curve.

4.3 | Suliciu's model

The corona phenomenon is simulated assuming that the current i_{co} drained transversally to ground by any elemental section, corresponding to the time derivative of the corona over-charge q_{co} , is given by

$$i_{\text{co}}(t) = \frac{dq_{\text{co}}}{dt} = \begin{cases} 0, & g_2(t) < 0 \\ g_2(t), & g_1(t) \leq 0 \leq g_2(t) \\ g_1(t) + g_2(t), & g_1(t) > 0 \end{cases} \quad (28)$$

where

$$g_p(t) = K_p [(C_p - C_{\text{geo}})(v(t) - V_p) - q_{\text{co}}(t)], \quad (29) \\ p = 1, 2,$$

and $C_2 > C_1 > C_{\text{geo}}$, and $V_1 > V_2 > 0$. Positive-valued K_1 and K_2 range between a few kHz and some MHz; however, the values of these parameters should be tuned to properly fit measured data; for a bundle of 4 conductors (each presenting a diameter of 3.05 cm), with equivalent geometric capacitance $C_{\text{geo}} = 17 \text{ pF/m}$, under voltage impulses ranging between 2.5/60 and 260/2300 μs , parameters to fit measured $q-v$ curves are [25, 45]: $C_1 = 31 \text{ pF/m}$, $C_2 = 66 \text{ pF/m}$, $V_1 = 463 \text{ kV}$, $V_2 = 434 \text{ kV}$, $k_1 = 1 \text{ MHz}$, $k_2 = 0.8 \text{ kHz}$.

5 | RESULTS AND DISCUSSION

We will refer to a 15 km long MTL (rated voltage 132 kV), whose conductors arrangement at the towers is depicted in Figure 2. Phase conductors, indicated P1, P2 and P3, closed on their characteristic impedance (computed for the corresponding lossless line) at the line terminations, are at heights $h_{P1} = 28$, $h_{P2} = 26$, and $h_{P3} = 24$ above a lossy ground with conductivity $\sigma_g = 0.01$ S/m and electric permittivity $\epsilon_g = 10\epsilon_0$. The shield wire (SW) is at height $h_{SW} = 33.5$ m and is grounded at both line terminations. Radii of the aluminium phase conductors and SW are, respectively, 1.58 and 0.58 cm.

5.1 | Fast-front voltage source

The parameters in Table 1, needed to include the reviewed models in Section 4, have been chosen in order to get $q-v$ curves similar in shape when a single conductor is fed by an ideal voltage source, which is given by the following Heidler's expression [46]:

$$v(t) = \frac{V_0}{\eta} \frac{\left(\frac{t}{\tau_1}\right)^n}{1 + \left(\frac{t}{\tau_1}\right)^n} \exp\left(-\frac{t}{\tau_2}\right), \quad (30)$$

where $\tau_1 = 0.63$ and $\tau_2 = 67.3$ μ s are time constants affecting the rise time and the half-to-peak values, which correspond, according to the definition given in [47], to 1.2 and 50 μ s, respectively; V_0 has been set to twice the inception voltage of a conductor of radius 1.58 cm, computed as in Equation (1), that is, $V_{inc} = 358.9$ kV with $m = 0.75$, $\delta = 1$, $f_p = 1$. η is the amplitude correction factor, whose expression may be found in [46]. Since the following results will deal with P1 being fed at the line left termination by a voltage source through a matched impedance, the parameters have been selected for a reference conductor at height $h = 28$ m, and radius $r_0 = 1.58$ cm.

In order to assess the validity of the code developed in the time domain, we display in Figure 3 the results for the MTL (in

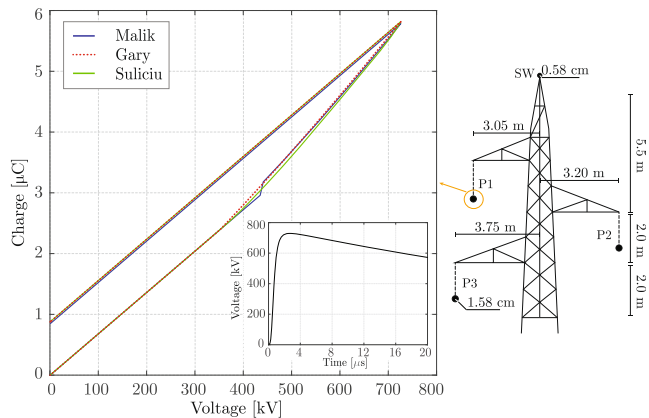


FIGURE 2 Arrangement and relevant geometric parameters of the conductors at the poles for the chosen MTL (rated voltage 132 kV)

Figure 2) at 0 km, and 1 km from the line left termination, in the absence of corona, computed with the implicit FDTD scheme and with a code in the frequency domain (followed by an inverse Fourier transform). Phase P1 is fed through a matching impedance by the aforementioned voltage source, with $V_0 = 4V_{inc}$. Negligible differences may be noticed, due to the implementation of the Prony method for the evaluation of losses in the time domain (computed following the approach presented in [6]). Unfortunately, the authors do not have measured data for the chosen configuration; however, this section is more focussed on analysing the consistency of results from the models when their parameters have been set to give similar $q-v$ curves, rather than validating their predicting capability, which will be addressed in the subsequent section.

Figure 4 show voltages-to-ground of the fed phase, that is, conductor P1, at 0 km, 1 km, and 7 km from the line left termination, evaluated with the three corona models. In light grey, voltage in the absence of corona is displayed as well; along with attenuation, a relevant reduction in propagation velocity may be observed at larger distances from the fed termination. Suliciu's and Gary's models result in satisfying agreement; differences with respect to Malik's model, which are negligible at 0 km, enhance increasingly at 1 km (Figure 4b) and 7 km (Figure 4c).

Explanation may be found from the analysis of Figure 5, in which $q-v$ curves evaluated for conductor P1 at 0, 1, and 7 km

TABLE 1 Parameters for the implementation of the corona models in Section 4

Suliciu	$C_1 = 8.9$ pF/m	$C_2 = 9.2$ pF/m
	$K_1 = 8$ MHz	$K_2 = 4$ MHz
	$V_1 = V_{inc}$	$V_2 = V_{inc}$
Malik	$\tau = 0.1$ μ s	$\alpha = 0.3$
Gary	$B = 1.121 + 6.8r_0$	

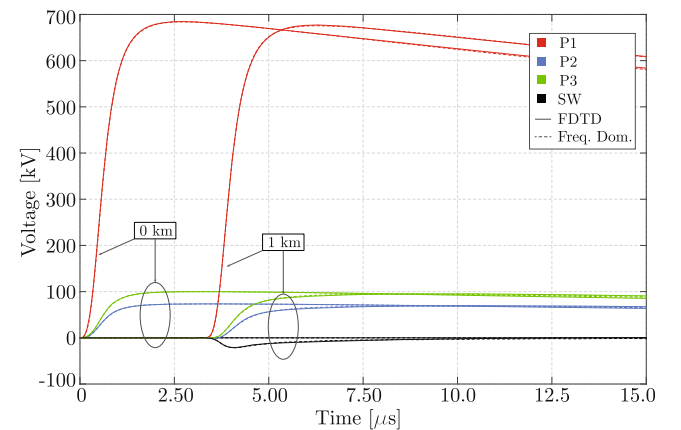


FIGURE 3 Comparison of results computed by the implicit FDTD scheme ($\Delta x = 4$ m, $\Delta t \approx 12$ ns) and by inverse Fourier Transform of frequency domain results for the line in Figure 1, in the absence of corona, P1 being fed by a 1.2/50 μ s voltage source

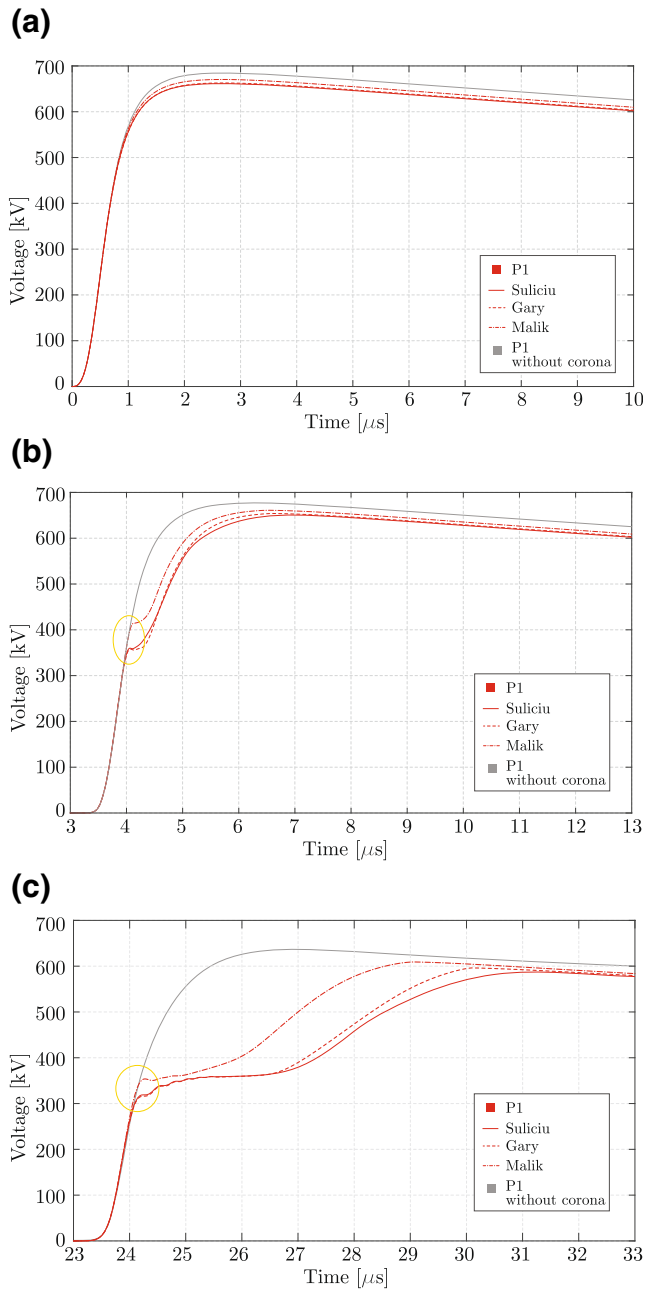


FIGURE 4 Conductor P1 voltage to ground at different distances from the line fed termination computed with the three corona models in Section 4, and $1.2/50 \mu\text{s}$ voltage source; (a) voltages at the line left termination; (b) voltages at 1 km from the left termination; (c) voltages at 7 km from the left termination

are depicted. While loops obtained from Suliciu's and Gary's models are comparable at the observed points along the line, the discontinuity in Malik's curves, due to the abrupt change of the corona equivalent radius, deserves some remarks. Reduced area of the charge-voltage loop at 7 km in Figure 5a compared to the corresponding area at 7 km in Figure 5b,c is consistent with the voltage less pronounced attenuation given by Malik's model. Reduction of the $q-v$ loop area is mainly due to the different voltage at which the charge discontinuity is located, which is at about 440 and 360 kV for 0 and 7 km, respectively.

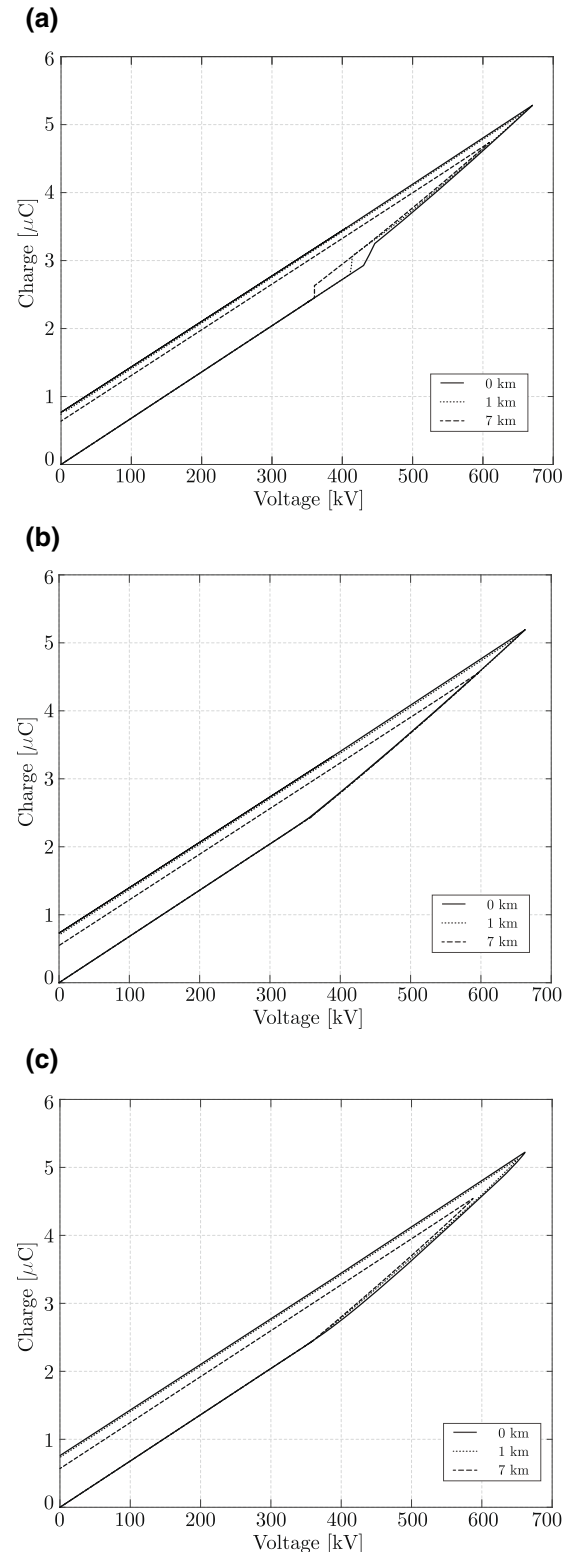


FIGURE 5 Hysteretic $q-v$ loops linked to voltage to ground of conductor P1 depicted in Figure 4, with $1.2/50 \mu\text{s}$ voltage source; (a) Malik's model; (b) Gary's model; (c) Suliciu's model

Due to the delay τ of the charge against time the inception voltage of the conductor is reached the first formation of corona over-charge occurs in correspondence with larger

voltage values at points closer to the voltage source; conversely, milder rates of voltage raise at larger distances, due to attenuation of high-frequency content of the travelling waves due to losses along the line, keep the discontinuity at lower voltage values, further reducing the q - v loop area. Its effect on surge propagation has been also highlighted in yellow in Figure 4b,c.

In Figure 6, we show voltages induced on the other conductors of the MTL; the results given by the implemented corona models differ more consistently at 7 km from the voltage source, as expected from the curves relative to the fed conductor at corresponding distances (Figure 4).

Figure 7 has been included in order to support Section 3.1 on the topic of the difficult numerical implementation of the dynamic capacitance approach with accuracy. The voltage to ground increment ΔV of conductor P1 at 7 km from the fed termination for the three implemented models, and the equivalent radius given by Malik's approach are displayed with different scale. The approach presented in Section 3.1 is based on the numerical computation of C_{dyn} as the ratio $\Delta q/\Delta V$. From Figure 7, it can be observed that after the corona inception, due to the abrupt increase of p.u.l line capacitance,

the line voltage $v(t)$ is oscillating and the ΔV crosses the 0 V reference line. Hence, the division may result in numerical problems and/or poor accuracy. The voltage-controlled current generator approach overcomes this problem, by direct evaluation of the corona current $i_{\text{co}}(t)$.

5.2 | Slow front voltage source

The results for a typical switching voltage wave, namely a 250/2500 μs impulse [47], have been included for comparison of corona effects on propagation with respect to previously discussed results for a fast-front surge. The parameters of the voltage source, feeding conductor P1 through a matching impedance, are $\tau_1 = 75.5 \mu\text{s}$, $\tau_2 = 3124 \mu\text{s}$, $n = 3$, and $V_0 = 4V_{\text{inc}}$. Voltages-to-ground of the fed conductor, that is, P1, at 0, 1, and 7 km from the line left termination are depicted in Figure 8, while voltages of conductors P2, P3, and of the SW are depicted, at the same observation points along the line, in Figure 9. For the same V_0 , corona holds minor impact on propagation, due to reduced front steepness of the voltage wave, that is, to smaller transversal corona currents (depending on dv/dt).

Furthermore, discrepancies between results from the three models on the shape of the travelling surge at growing distances from the fed termination reduce to less than 1% of the peak value (in the absence of corona) at 7 km. This point might be addressed through inspection of q - v curves relative to the fed conductor, computed through the implemented corona models, and included in insight of Figure 8. Charge discontinuity in the loops from Malik's model, which has been recognised as the main cause for growing results differences with other models at larger distances from the feeding point, is not sensibly affected by position of the observed point along the line (contrary to results in Figure 5a); in fact, with the current switching impulse, the impact of the time delay τ on the loop shape is strongly limited, due to the less steep harsh front of the surge, leading to results comparable with other models.

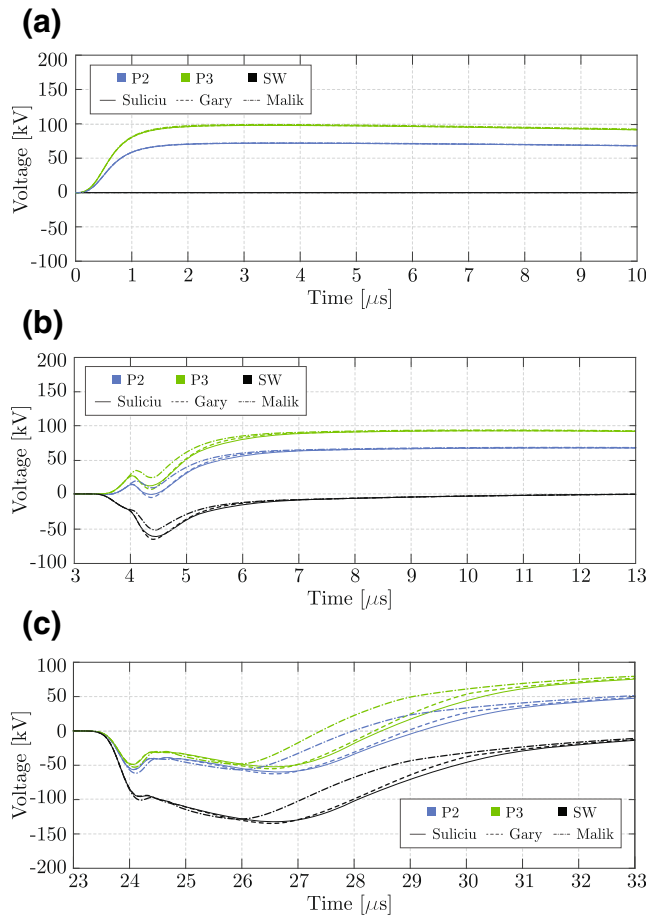


FIGURE 6 Voltages-to-ground induced on conductors P2, P3, and on the SW at different distances from the line fed termination, computed with the three corona models in Section 4, and 1.2/50 μs voltage source; (a) voltages at the line left termination; (b) voltages at 1 km from the left termination; (c) voltages at 7 km from the left termination

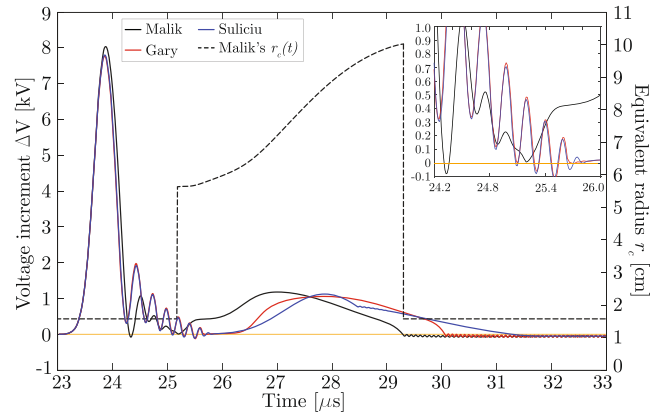


FIGURE 7 Increment $\Delta V(t)$ of voltage of P1 at 7 km from the fed termination for the three models, and $r_c(t)$ by Malik's approach, under the same conditions of Figure 4c

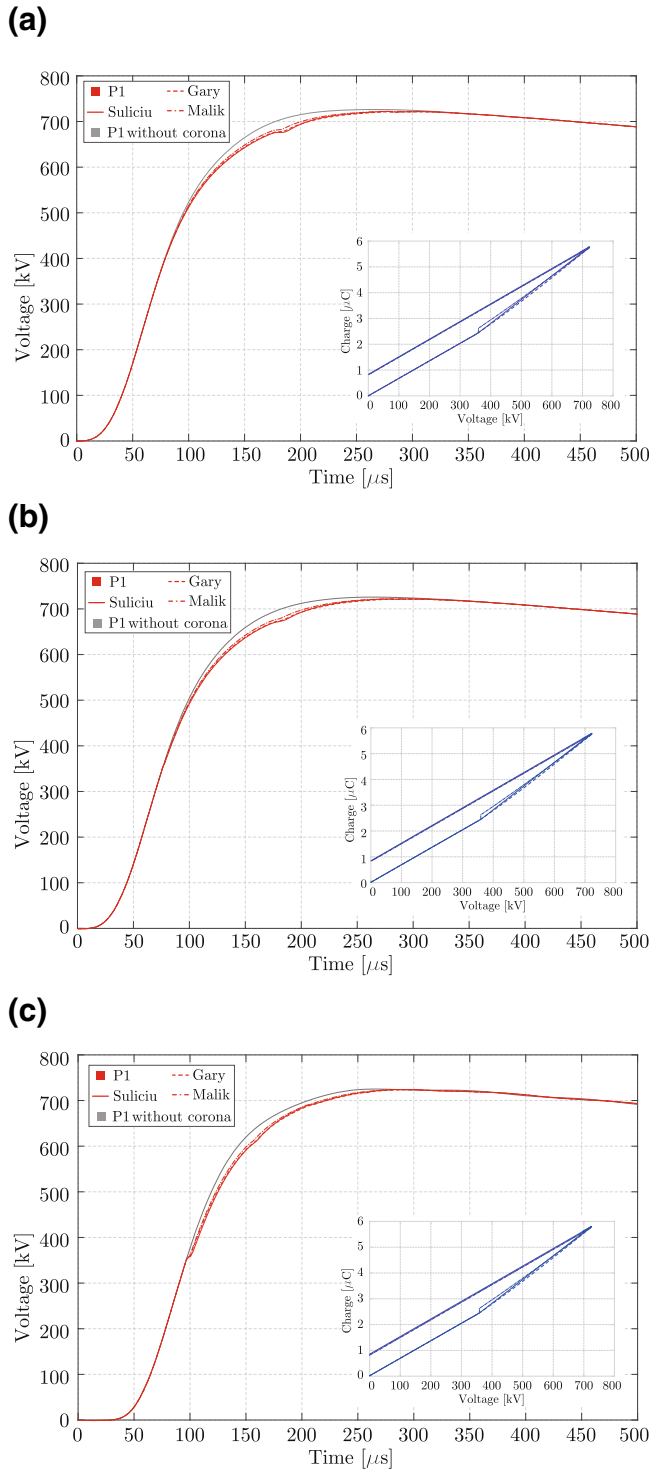


FIGURE 8 Conductor P1 voltage to ground at different distances from the line fed termination computed with the three corona models in Section 4, and 250/2500 μ s voltage source; (a) voltages at the line left termination; (b) voltages at 1 km from the left termination; (c) voltages at 7 km from the left termination

In Figure 9, voltages produced on the other conductors are displayed in a different scale, at observation points corresponding to those in Figure 8, and compared to voltages produced in the absence of corona (in light grey). Reflections

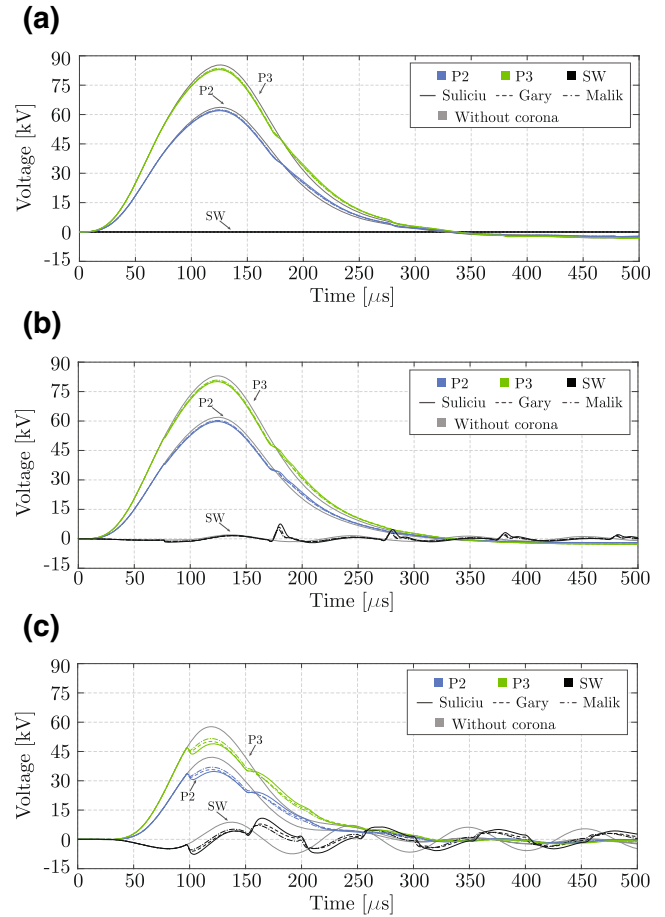


FIGURE 9 Voltages-to-ground induced on conductors P2, P3, and on the SW at different distances from the line fed termination, computed with the three corona models in Section 4, and 250/2500 μ s voltage source; (a) voltages at the line left termination; (b) voltages at 1 km from the left termination; (c) voltages at 7 km from the left termination

at the line terminations are more apparent when corona discharge is simulated. This phenomenon is linked to an enhancement in the already existing mismatch between the constant line adopted terminations, and the characteristic impedance of the lossy line; indeed, corona further deviates the line capacitive behaviour from its linear one, only associated with the conductors arrangement and geometry. In particular, with reference to voltages in Figure 9a, no deviation from reference voltages in grey (in the absence of corona) can be observed until corona inception for conductor P1 occurs at around 73 μ s; at later times, enhanced reflections are visible at intervals of about 100 μ s, corresponding to the time necessary for the traveling wave to go back to the feeding point, after reflection at the right termination. Analogous observations can be made for outputs in Figure 9b,c, considering suitable time intervals for the expected reflections from the line endpoints.

Finally, $q-v$ models in the literature, from which suitable expressions for i_{co} have been derived, are frequently tailored on experimental data referring to different configurations

from ones involving transmission lines; in fact, they often refer to short cylindrical conductors fed by known voltage sources, the charge being considered as the output of a system with a given voltage as input; instead, in propagation studies, corona over-charge developed in response to voltage has an influence on voltage waveform itself, due to the reduced propagation velocity and additional losses introduced by the hysteretic capacitive behaviour of the conductor under corona, which are not predictable a priori. This is not a secondary aspect to consider when trying to include corona in FDTD schemes through the dynamic capacitances matrix approach; while models are based on conductors fed by voltage sources that are strictly monotonically increasing until their peak value, this might not be the case in applications involving propagation: delays associated with corona discharge may result in intervals with very slow, or no variation in conductor-to-ground voltages at large distances from the source (e.g. results from Suliciu's model in Figure 4c, at about 26 μ s), leading to a numerically unfriendly, undeterminate form of the ratio dq/dv . Furthermore, charge given by models relying on a q - v time dispersive relation are expected to depend on the voltage derivative, that is, to present different hysteretic loops for different excitation voltages [48]. This further justifies the agreement between Gary's and Suliciu's approaches that model charge as an instantaneous non-linear response of the system to a voltage input, and, on the other hand, the discrepancy with Malik's model, which relies on the sum of an instantaneous linear response (i.e. $C_{\text{geo}}v(t)$ in Equation (22)) and a non-linear delayed one (i.e. the right side member in Equation (22), except for $C_{\text{geo}}v(t)$).

Computational time for results associated with the 15-km line discussed here, $\Delta t \approx 12$ ns, $\Delta x = 4$ m, with the fast-front voltage source, was approximately 3 min on a desktop Intel computer.

5.3 | Numerical implementation against experimental data

In Figure 10, we show how the parameters of the models may be easily set to match with good agreement with an experimental q - v loop [17], measured applying a 10/75 μ s voltage wave to the conductor in the figure insight.

Corona models in Section 4, with parameters in Table 1 and $\Delta t \approx 2.7$ ns, have been additionally tested with a different waveform, and adopted to reproduce experimental data.

The first set of data is found in the literature from Gary [49]; voltage to ground is measured for a three conductors test line, with horizontal configuration, arranged as depicted in the insight of Figure 11. The line is 65 km long, short circuited at the right termination; at the left termination, the external conductor C1 is fed by a voltage source by means of an unmatched impedance, resulting, at the sending end, in the following waveform (expressed in kV, with time in μ s, and including a typographic correction) [49]:

$$v(t) = 850 \left[0.988 e^{-0.123t} - 1.051 e^{-4.1t} \sin(12.3t + 70^\circ) \right]. \quad (31)$$

The results computed by means of the implicit FDTD scheme are compared to the measured voltage of the fed conductor C1, at 1 and 3 km from the left termination. Uncertainties related to the ground electrical properties ($\sigma_g = 250$ S/m, and $\epsilon_g = 10\epsilon_0$ are assumed), and impedance of the feeding source, produce a difference of about 6% and 2% of the peak values computed by the FDTD algorithm with respect to the corresponding peak values measured at 1 and 3 km. Sets of parameters employed for the models have not been changed from those displayed in Table 1, which still result in good agreement with the numerical results with experimental data involving this first configuration.

The models have been additionally employed to reproduce voltage surge measured by Wagner, Gross and Lloyd along a test line located in Ohio [9]. Data chosen here for comparison refer to an ACSR (steel-reinforced aluminium conductor) single conductor with radius $r_0 = 25$ mm and about 2.2 km long, fed by a surge generator; at the end termination, the line is closed on a resistor with resistance approximately equal to the line characteristic impedance (about 439 Ω). Starting from the description of the original test site, the geometrical configuration under analysis is displayed in the insight of Figure 12. As to the properties of the ground, the relative electrical permittivity is set to 10 while the value of 500 $\Omega \cdot m$ is chosen as the average ground resistivity considering the average values given by the World Atlas of Ground Conductivities [50] in the test site area. Since the analytical expression for the voltage waveform applied is not given, a double exponential approximation in the least square sense is found to match the voltage curve measured at the fed termination (expressed in kV):

$$v(t) = 1551.5 f_p \left(e^{-\frac{t}{\tau_1}} - e^{-\frac{t}{\tau_2}} \right), \quad (32)$$

with

$$f_p = [\exp(-t_m/\tau_1) - \exp(-t_m/\tau_2)]^{-1} \quad (33)$$

$$t_m = \frac{\tau_1 \tau_2}{\tau_1 - \tau_2} \log(\tau_1/\tau_2), \quad (34)$$

and $\tau_1 = 6.64$ μ s, $\tau_2 = 3.61$ μ s. The parameters required by the different models have been chosen in order to better match the experimental data measured at 660 m, 1300 m from the fed termination, and at the line end point; the values adopted are $\tau = 0.1$ μ s, and $\alpha = 0.3$ for Malik's model; $B = 1.212 + 6.8r_0$ for Gary's model; $C_1 = 10$ pF/m, $C_2 = 13$ pF/m, $K_1 = 9$ MHz, $K_2 = 4$ MHz, and $V_1 = V_2 = V_{\text{inc}} \approx 489.9$ kV for Suliciu's model. Comparing the curves in Figure 12, the effect of Malik's delay time τ , already underlined in Sec. 5.1, contributes to differentiate

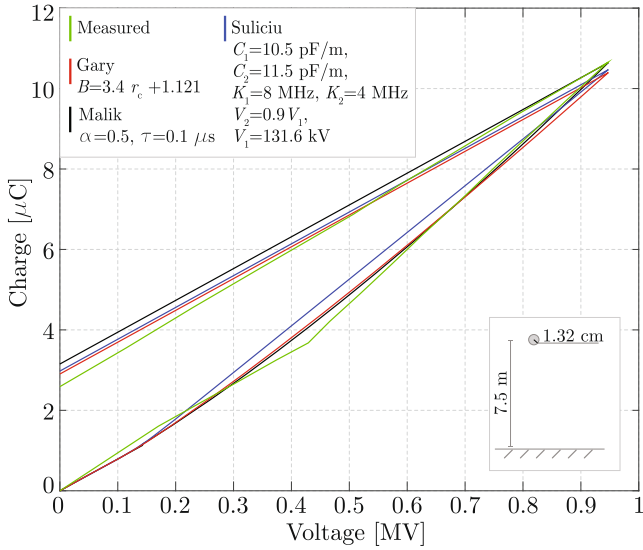


FIGURE 10 Example of the choice of suitable models parameters to reproduce a measured $q-v$ curve [17]

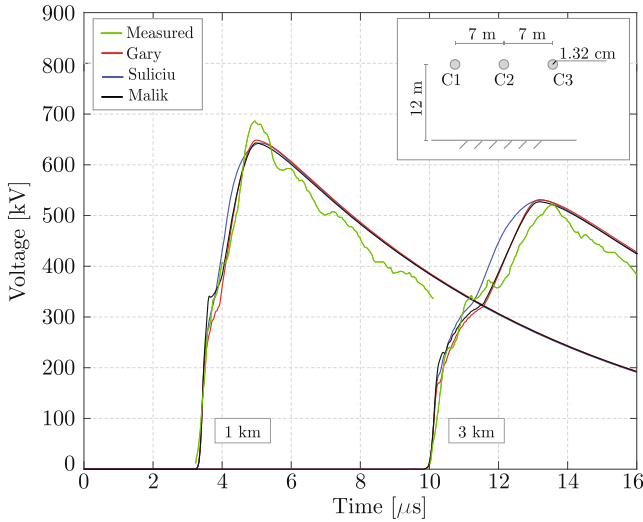


FIGURE 11 Comparison of results from corona models in Section 4 and measured voltages for the fed conductor C1 of the test line in insight [49].

Malik's results from those computed with the other models. Instead, with Gary's and Suliciu's approaches, more accurate results in terms of voltage derivative at the front and peak value of the surge along the line may be reached; the results confirm the versatility of Suliciu's model, due to the higher degrees of freedom available, that is, the larger number of parameters which can be adjusted and set to match measured data.

In Figure 13, we show voltages computed for conductor C1 of the line displayed in insight (with total length equal to 1410 m), compared to the experimental data from [51] (in Japanese). Conductor C1 is closed at the end termination on a resistive impedance of 490Ω , whereas conductor C2 is open at both terminations. Ground electrical permittivity is

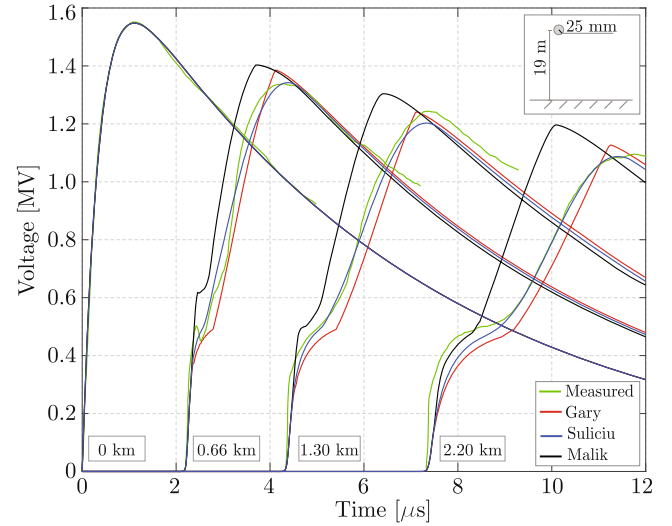


FIGURE 12 Comparison of results from corona models in Section 4 and measured voltages for the fed conductor in insight at different distances from the fed termination [9]

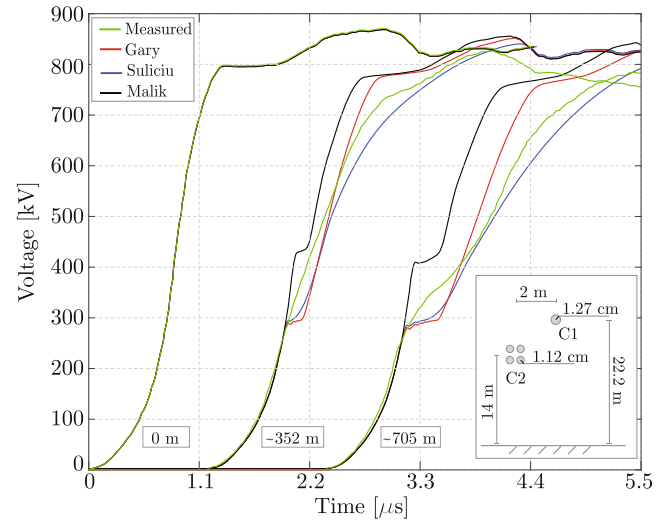


FIGURE 13 Comparison of results from corona models in Section 4 and measured voltages for the fed conductor C1 in insight at different distances from the fed termination [51]

set to 10, and ground resistivity is set to $100 \Omega \cdot m$ [52]. The applied voltage corresponds to the waveform displayed for 0 km. Since an analytical expression is not given for the applied voltage at 0 km, this was obtained from interpolation of results available in [51, 52], and imposed at the fed termination of C1. The parameters adopted for the implementation of the models are left unchanged from the previous configuration, updating the inception voltage of conductor C1 to the value $V_{inc} \approx 294.2$ kV. Figure 13 endorses the versatility of Suliciu's model that presents again the best agreement, yet the overall results prove that the simulation of corona phenomena requires an accurate setting of fundamental model parameters.

6 | CONCLUSION

Non-linearity and non-uniformity derived from corona discharge along MTLs have been successfully included in an implicit FDTD updating scheme. The possibility of including corona by the modification of the matrix of potential coefficients locally, for points along the line at which at least one conductor enters corona, has been taken into account; the more numerically friendly choice of plugging equivalent voltage-controlled current generators along the line has been implemented, due to its general validity when dealing with models that introduce a time delay between corona charge formation and voltage.

Three different approaches for simulating corona discharge, that is, Malik's, Gary's and Suliciu's models, have been reviewed in detail and implemented. The relationship between q - v loops' shapes, computed through these corona models, and steepness of the voltage surge have been discussed when dealing with propagation phenomena, also referring to the effects induced on non-fed conductors of the line. Matching of the hysteretic loops for the voltage applied at the line termination is shown not to lead to sufficiently coherent results among the physics-based model (i.e. Malik's model) and empirical models (Gary's and Suliciu's models) at growing distances from the feeding point, especially in the case of fast-front voltage impulses.

We introduce an alternative approach to include the influence of corona discharge in numerical codes studying propagation along multiconductor transmission lines. In addition, we highlight the strong dependence of the computed results on the chosen corona model. We show that the implementation of different models does not lead to equivalent results, with the same line configuration and source. Hence, the choice of a specific corona model may lead to results whose general validity is questionable; research is needed in the direction of finding a model of general applicability.

DATA AVAILABILITY STATEMENT

Research data are not shared.

ORCID

Rodolfo Araneo  <https://orcid.org/0000-0003-4771-9584>

REFERENCES

- Hileman, A.R.: *Insulation Coordination for Power Systems*. CRC Press, London (1999)
- Andreotti, A., et al.: An accurate approach for the evaluation of the performance of overhead distribution lines due to indirect lightning. *Electr. Power Syst. Res.* 186, 106411 (2020)
- Thang, T.H., et al.: FDTD simulation of insulator voltages at a lightning-struck tower considering ground-wire corona. *IEEE Trans. Power Del.* 28(3), 1635–1642 (2013)
- Araneo, R., et al.: Utilization of underbuilt shield wires to improve the lightning performance of overhead distribution lines hit by direct strokes. *IEEE Trans. Power Del.* 35(4), 1656–1666 (2020)
- Liu, X., et al.: Fast evaluation of lightning-induced voltages of overhead line and buried cable considering the lossy ground. *IET Sci. Meas. Technol.* 13(1), 67–73 (2019)
- Araneo, R., Celozzi, S.: Direct time-domain analysis of transmission lines above a lossy ground. *IEEE Proc. Sci. Meas. Technol.* 148(2), 73–79 (2001)
- Said, A., Anane, Z.: Corona lightning overvoltage analysis for a 500 kV hybrid line. *IET Gener. Transm. Distrib.* 14(4), 532–541 (2020)
- Peek, F.W.: *Dielectric Phenomena in High Voltage Engineering*. McGraw-Hill Book Company Incorporated (1920)
- Wagner, C.F., Gross, I.W., Lloyd, B.L.: High-voltage impulse tests on transmission lines. *Trans. Am. Inst. Electr. Eng. Part III.* 73(2), 196–210 (1954)
- Xu, Z., Hei, G.: Rectangular spiral antenna with a Hilbert unit for detecting corona discharge in overhead lines. *IEEE Sensors J.* 21(2), 930–936 (2021)
- Clade, J.J., Gary, C.H., Lefevre, C.A.: Calculation of corona losses beyond the critical gradient in alternating voltage. *IEEE Trans. Power Appar. Syst.* PAS-88(5), 695–703 (1969)
- Lowke, J.J., Alessandro, D.F.: Onset corona fields and electrical breakdown criteria. *J. Phys. Appl. Phys.* 36(21), 2673–2682 (2003)
- Noda, T., et al.: Charge-voltage curves of surge corona on transmission lines: Two measurement methods. *IEEE Trans. Power Del.* 18(1), 307–314 (2003)
- Pearson, J.D., Trevena, D.H.: Definition of capacitance. *J. Electron. Control.* 6(1), 74–74 (1959)
- Anane, Z., Bayadi, A., Huang, K.: Distortion phenomena on transmission lines using corona modeling ATP/EMTP. *IEEE Trans. Dielectr. Electr. Insul.* 25(2), 383–389 (2018)
- Bousiou, E.I., Mikropoulos, P.N., Zagkanas, V.N.: Corona inception field of typical overhead line conductors under variable atmospheric conditions. *Electr. Power Syst. Res.* 178, 106032 (2020)
- Li, X.R., Malik, O.P., Zhao, Z.D.: A practical mathematical model of corona for calculation of transients on transmission lines. *IEEE Power Eng. Rev.* 9(4), 75–75 (1989)
- Zhang, X., et al.: An improved fluid model study: the effect of cross-section geometry on positive corona discharge on dc transmission conductors. *IEEE Trans. Plasma Sci.* 48(8), 2846–2855 (2020)
- Huang, K., Zhang, X., Tao, S.: Electromagnetic transient analysis of overhead lines including corona and frequency-dependence effects under damped oscillation surges. *IEEE Trans. Power Del.* 33(5), 2198–2206 (2018)
- Cooray, V.: Charge and voltage characteristics of corona discharges in a coaxial geometry. *IEEE Trans. Dielectr. Electr. Insul.* 7(6), 734–743 (2000)
- De Jesus, C., Correia de Barros, M.T.: Modelling of corona dynamics for surge propagation studies. *IEEE Trans. Power Del.* 9(3), 1564–1569 (1994)
- Huang, K., Zhang, X., Xiao, X.: Modelling of the corona characteristics under damped oscillation impulses. *IET Gener. Transm. Distrib.* 10(7), 1648–1653 (2016)
- Inoue, A.: Propagation analysis of overvoltage surges with corona based upon charge versus voltage curve. *IEEE Trans. Power App. Syst.* PAS-104(3), 655–662 (1985)
- Gary, C., Dragan, G., Langu, I.: Impulse corona discharge energy around the conductors. In: *IEEE Industry Applications Society Annual Meeting*, vol. 1, pp. 922–924. IEEE (1990)
- Mihalescu-Suliciu, M., Suliciu, I.: A rate type constitutive equation for the description of the corona effect. *IEEE Trans. Power App. Syst.* PAS-100(8), 3681–3685 (1981)
- Podporokin, G.V., Sivaev, A.D.: Lightning impulse corona characteristics of conductors and bundles. *IEEE Trans. Power Del.* 12(4), 1842–1847 (1997)
- Skilling, H.H., Dykes, P.D.K.: Distortion of traveling waves by corona. *Trans. Am. Inst. Electr. Eng.* 56(7), 850–857 (1937)
- Umoto, J., Hara, T.: Numerical analysis of surge propagation on single-conductor systems considering corona losses. *Electr. Eng. Jpn.* 89(5), 21–28 (1969)
- Carneiro, S., Marti, J.R.: Evaluation of corona and line models in electromagnetic transients simulations. *IEEE Trans. Power Del.* 6(1), 334–342 (1991)
- Lee, K.C.: Non-linear corona models in an electromagnetic transients program (EMTP). *IEEE Trans. Power Appar. Syst.* PAS-102(9), 2936–2942 (1983)

31. Maruvada, P.S., Nguyen, D., Hamadani Zadeh, H.: Studies on modeling corona attenuation of dynamic overvoltages. *IEEE Trans. Power Del.* 4(2), 1441–1449 (1989)
32. Motoyama, H., Ametani, A.: Development of a linear model for corona wave deformation and its effects on lightning surges. *Electr. Eng. Jpn.* 107(2), 98–106 (1987)
33. Araneo, R., et al.: Comparison of corona models for computing the surge propagation in multiconductor power lines. In: 2016 IEEE 16th International Conference on Environment and Electrical Engineering (EEEIC), pp. 1–6. (2016)
34. Stracqualursi, E., et al.: Analysis of metal oxide varistor arresters for protection of multiconductor transmission lines using unconditionally-stable Crank–Nicolson FDTD. *Energies.* 13(8), 2112 (2020)
35. Brignone, M., et al.: On the stability of FDTD - based numerical codes to evaluate lightning - induced overvoltages in overhead transmission lines. *IEEE Trans. Electromagn. Compat.* 62(1), 108–115 (2020)
36. Wang, L., et al.: The splitting Crank-Nicolson scheme with intrinsic parallelism for solving parabolic equations. *J. Function Spaces.* 2020, 8571625 (2020)
37. Yamazaki, K., Olsen, R.G.: Application of a corona onset criterion to calculation of corona onset voltage of stranded conductors. *IEEE Trans. Dielectr. Electr. Insul.* 11(4), 674–680 (2004)
38. Mikropoulos, P., Zagkanas, V.: Impulse corona inception in the coaxial cylindrical electrode arrangement in air: effects of the steepness of the applied voltage. In: Proc. 18th International Symposium on High Voltage Engineering (2013)
39. Paul, C.R.: *Analysis of Multiconductor Transmission Lines.* John Wiley and Sons (2008)
40. Rachidi, F., Nucci, C.A., Ianoz, M.: Transient analysis of multiconductor lines above a lossy ground. *IEEE Trans. Power Del.* 14(1), 294–302 (1999)
41. Stracqualursi, E., et al.: Unconditionally stable implicit schemes for transient analysis of lossy multiconductor lines. *IEEE Trans. Electromagn. Compat.* 63(2), 640–644 (2021)
42. Florea, G., et al.: Considerations on the line capacitance under surge corona discharge. In: International Symposium on Electromagnetic Compatibility - EMC EUROPE, pp. 1–6. IEEE (2012)
43. Liu, X., et al.: Modified field-to-line coupling model for simulating the corona effect on the lightning induced voltages of multi-conductor transmission lines over a lossy ground. *IET Gener. Transm. Distrib.* 11(7), 1865–1876 (2017)
44. Monrolin, N., Praud, O., Plouraboué, F.: Revisiting the positive DC corona discharge theory: Beyond Peek's and Townsend's law. *Phys. Plasmas.* 25(6), 063503 (2018)
45. Maruvada, P.S., Menemenlis, H., Malewski, R.: Corona characteristics of conductor bundles under impulse voltages. *IEEE Trans. Power Appar. Syst.* 96(1), 102–115 (1977)
46. Gamera, W.R., et al.: Current waveforms for lightning simulation. *IEEE Trans. Electromagn. Compat.* 54(4), 880–888 (2012)
47. IEEE Std 4-2013: IEEE standard for High-Voltage Testing Techniques. IEEE (2013)
48. Bousiou, E., Mikropoulos, P.: Experimental investigation on corona charge-voltage characteristics in the coaxial configuration under lightning impulse voltages. In: 2018 IEEE International Conference on High Voltage Engineering and Application (ICHVE), pp. 1–4. IEEE (2018)
49. Gary, C.: Attenuation of Travelling Waves Caused by Corona. CIGRE Report 22-13. (1978)
50. ITU-R: World Atlas of Ground Conductivities. (1999)
51. Inoue, A.: Study on propagation characteristics of high-voltage traveling waves with corona discharge. CRIEPI (Cent. Res. Inst. Electr. Power Ind.) Rep. 114 (1983)
52. Thang, T.H., et al.: FDTD simulation of lightning surges on overhead wires in the presence of corona discharge. *IEEE Trans. Electromagn. C.* 54(6), 1234–1243 (2012)

How to cite this article: Stracqualursi, E., Araneo, R., Andreotti, A.: The impact of different corona models on FD algorithms for the solution of multiconductor transmission lines equations. *High Volt.* 1–14 (2021). <https://doi.org/10.1049/hve2.12143>